



Introducing SlideforMap; a probabilistic finite slope approach for modelling shallow landslide probability in forested situations

Van Zadelhoff Feiko¹, Albaba Adel¹, Cohen Denis², Phillips Chris³, Schaepli Bettina⁴, Dorren Lucas Karel Agnes^{1,5}, and Schwarz Massimiliano^{1,5}

¹Bern University of Applied Sciences - HAFL, Länggasse 85, CH-3052 Zollikofen, Switzerland

²COSCI Ltd.

³Manaaki Whenua - Landcare Research, Lincoln, New Zealand

⁴Institute of Geography (GIUB) & Oeschger Centre for Climate Change Research (OCCR), University of Bern, 3012 Bern, Switzerland

⁵Int. ecorisQ Association, P.O. Box 2348, 1211 Geneva 2, Switzerland

Correspondence: Van Zadelhoff F.B. (feiko.vanzadelhoff@bfh.ch)

Abstract. Worldwide, shallow landslides repeatedly pose a risk to infrastructure and residential areas. To analyse and predict the risk posed by shallow landslides, a wide range of scientific methods and tools to model shallow landslide probability exist for both local and regional scale. However, most of these tools do not take the protective effect of vegetation into account. Therefore, we developed SlideforMap (SfM), which is a probabilistic model that allows for a regional assessment of shallow landslide probability while considering the effect of different scenarios of forest cover, forest management and rainfall intensity. SfM uses a probabilistic approach by distributing hypothetical landslides to uniformly randomized coordinates in a 2D space. The surface areas for these hypothetical landslides are derived from a distribution function calibrated from observed events. For each randomly generated landslide, SfM calculates a factor of safety using the limit equilibrium approach. Relevant soil parameters, i.e. angle of internal friction, soil cohesion and soil depth, are assigned to the generated landslides from normal distributions based on mean and standard deviation values representative for the study area. The computation of the degree of soil saturation is implemented using a stationary flow approach and the topographic wetness index. The root reinforcement is computed based on root proximity and root strength derived from single tree detection data. Ultimately, the fraction of unstable landslides to the number of generated landslides, per raster cell, is calculated and used as an index for landslide probability. Inputs for the model are a digital elevation model, a topographic wetness index and a file containing positions and dimensions of trees. We performed a calibration of SfM for three test areas in Switzerland with a reliable landslide inventory, by randomly generating 1000 combinations of model parameters and then maximising the Area Under the Curve (AUC) of the receiver operation curve (ROC). These test areas are located in mountainous areas ranging from 0.5 – 7.5 km², with varying mean slope gradients (18 - 28°). The density of inventoried historical landslides varied from 5 – 59 slides/km². AUC values between 0.67 and 0.92 indicated a good model performance. A qualitative sensitivity analysis indicated that the most relevant parameters for accurate modeling of shallow landslide probability are the soil depth, soil cohesion and the root reinforcement. Further, the use of single tree detection in the computation of root reinforcement significantly improved model accuracy compared to



the assumption of a single constant value of root reinforcement within a forest stand. In conclusion, our study showed that the approach used in SfM can reproduce observed shallow landslide occurrence at a catchment scale.

keywords: mountain forest, shallow landslide probability, probabilistic modelling, single tree detection, root reinforcement

25

1 Introduction

Landslides pose serious threats to inhabited areas world-wide. They are the cause of 17% of the fatalities due to natural hazards in the period of 1994- 2013 (Kjekstad and Highland, 2009). Average annual monetary losses over the period of 2010 - 2019 are approximately 25 billion US dollars (Munich RE, 2018). In addition, Swiss Re Institute (2019) notes a significant increase in damages by hydrologically related natural hazards over the past 5 years, including hydrologically-triggered shallow landslides. This has been attributed to increased urbanization in risk-prone areas and to an increase in heavy rainfall events. Furthermore, Swiss Re Institute (2019) notes that the modelling of shallow landslides is underdeveloped compared to the severity of the danger they pose. In mountainous regions, landsliding is a prominent natural hazard. For instance, in the alpine parts of Switzerland, 74 people have died as a result of landslide events between 1946 and 2015 (Badoux et al., 2016). The annual cost of landslide protective measures alone is approximately 15 million CHF each year (Dorren and Sandri, 2009). No distinction is made between deep-seated and shallow landslides in these numbers. Rain induced shallow landslides are one of the most important and dangerous types of mass movement in mountainous regions (Varnes, 1978). Fortunately, improvements in hazard assessment have significantly decreased the number of shallow landslide related deaths over the past decades (Badoux et al., 2016). This general trend is also supported by long-term data (Munich RE, 2018). The fatality decrease is related to better organizational measures regarding hazards, such as warning based evacuations and road closures. Biological measures, such as management of protection forests, also play a role in mitigation of natural hazards. The latter role is especially important for (shallow) landslides, rockfall, snow avalanches and debris flows (Corominas et al., 2014). Shallow landslide probability has been modelled mostly using a deterministic approach ((Corominas et al., 2014). An example of a deterministic approach is the SHALSTAB model Dietrich and Montgomery (1998).

In recent decades, the development of probabilistic models and statistical methods has improved model performance for quantifying landslide probability and the interpretation of their results (Corominas et al., 2014). In statistical methods (e.g. Baeza and Corominas, 2001), there is no explicit accounting of physical processes. In contrast, probabilistic methods take physical processes into account and additionally quantify the reliability of the results considering the probability distribution of values of one or more input parameters (Salvatici et al., 2018). Generally, these models perform better than deterministic ones (Park et al., 2013; Zhang et al., 2018), likely due to natural landslides having a mode of movement significantly controlled



by internal inhomogeneities and discontinuities in the soil (Varnes, 1978). These control mechanisms are unpredictable at small-scales, making it hard for deterministic models to identify exact locations of instabilities. Below we will go into more detail on the initiation of shallow landslides.

55 Initiation of instability is, in fact, a process that combines mechanical and hydrological processes on different spatial and temporal scales and can thereby be very localized, with successive movement increasing the magnitude of the event (Varnes, 1978). In alpine environments, instabilities are typically triggered by rainfall, leading to soil wetting and ensuing increase of pore pressure, which destabilizes the soil and can then initiate soil movement. An increase in pore pressure can build up in minutes to months following a rainfall event (Iverson, 2000), where rapid pore pressure changes are attributed to macro-
60 pore flow and slow pore pressure changes to the matrix water flow. The higher the hydraulic conductivity of the soil, the faster pore pressure changes can develop (Iverson, 2000). Theoretically, a landslide resulting from a local instability could then continue indefinitely if the slope remains inclined and the shear resistance is low (Varnes, 1978). In reality, however, the passive earth pressure at the bottom of the triggering zone reacts with a resisting force, contributing thereby to landslide stabilisation (Schwarz et al., 2015; Cislighi et al., 2018). It is important to note here that the passive earth pressure is activated in a later
65 phase of the triggering of a shallow landslide and should not be added to active earth pressure or tensile forces acting along the upper half of the shallow landslide (Cohen and Schwarz, 2017).

The reaction of pore pressure to rainfall is variable and highly dependent on soil type. Pore pressure development has been studied experimentally. A key study is the work of Bordoni et al. (2015) in which in-situ measurements were taken on a slope with clayey–sandy silt and clayey–silty sand soils that experienced a shallow landslide. They showed that intense rainfall and a
70 rapid increase of pore pressure were the triggering factors of the landslide. Over the duration of the measurements, comparable saturation degrees have been reached both during prolonged and during intense rainfall events. In this case however, prolonged rainfall did not result in the pore pressure required to trigger a shallow landslide. Similar behaviour has been observed in an artificially triggered landslide in Rüdlingen (CH) (Askarinejad et al., 2012; Lehmann et al., 2013; Askarinejad et al., 2018). In the first wetting phase (in the year 2008), homogeneously induced rainfall with a duration of 3 days, an accumulated rainfall of
75 1700 mm and a peak intensity of 35 mm/hr, induced a maximum pore water pressure of 2 kPa at 1.2 m soil depth, resulting in no landslide. Whereas, in the second phase of the experiment (2009), the rainfall was heterogeneous. With a maximum intensity of 50 mm/hr in the upper part of the slope that induced an increase of pore water pressure up to 5 kPa at 1.2 m soil depth, resulting in the triggering of a shallow landslide. The triggering was reached after 15 hours with a cumulative rainfall of 150 mm. In addition, a computational study by Li et al. (2013) showed that at a high rainfall intensity (80 mm/hr), the pore water pressure at
80 a depth of 1 m reached a constant value within 1 hour. For a lower intensity of 20 mm/hr, this took approximately 3 hours. This shows that landslide triggering is related to a fast build up of pore water pressure proportional to rainfall intensity. The work of Wiekenkamp et al. (2016), suggests that preferential flow dominates the runoff in a heterogeneous catchment during extreme precipitation events. Water can move downslope very rapidly through macropores (in experimental conditions) under both saturated and unsaturated conditions (Mosley, 1982). The role of macropores can be very strong in a closed soil structure or in
85 presence of shallow impermeable bedrock, where macropore control of the soil hydrological behavior can be very pronounced. Further examples of the influence of macropores on hillslope hydrology in various soil types are presented in the work of



Weiler and Naef (2003); Bodner et al. (2014); Wiekenkamp et al. (2016). Additionally, Torres et al. (1998) demonstrates the strong role of macropore governed preferential flow paths for landslide triggering in an artificial rain experiment in a loamy sandy soil.

90 Besides hydrology, slope and soil characteristics, vegetation plays a key role in landslide triggering (Salvatici et al., 2018; Corominas et al., 2014; Greenway, 1987; González-Ollauri and Mickovski, 2014). Among other possible vegetation effects, root reinforcement, mobilized during soil movement, is an essential component (Greenway, 1987; Schwarz et al., 2010). It is a leading factor in the failure criterion for many vegetated slopes (Dazio et al., 2018). In modelling studies, the influence of root reinforcement on slope stability is often quantified as an apparent added cohesion (Wu et al., 1978; Borga et al., 95 2002). This apparent cohesion in turn can be added in the limit equilibrium computation of a Safety Factor (SF). Using a Monte Carlo approach of this method, it was found that the SF can gain up to 37% stability from including vegetation root reinforcement (Zhu et al., 2017). In another study in New Zealand, trees showed an effect on soil stability up to 11 meter away from their position and had the ability to prevent 70% of instability events (Hawley and Dymond, 1988). Computational research furthermore shows that root reinforcement by the larger roots is dominant over the smaller roots, even though they are 100 far less numerous (Vergani et al., 2014).

The planting pattern and management of the vegetation can have a profound effect on root reinforcement and thus on slope stability (Sidle, 1992). Therefore a detailed approach to vegetation modelling is important. Root reinforcement can be subdivided into two major components: Basal root reinforcement and lateral root reinforcement. Basal root reinforcement is the anchoring of tree roots through the sliding plane into the deeper soil. Lateral root reinforcement is the reinforcement from roots 105 on the edges of the potential slide that stick into the soil outside of the potential slide (Schwarz et al., 2010). In exchange, the mechanical influence of vegetation weight on slope stability is often considered negligible (Reinhold et al., 2009). In current shallow landslide probability modelling, root reinforcement is generally modelled in a simplified way. This limits the types of forest management practices that can be evaluated. In order to overcome this, we developed a shallow landslide probability model, named SlideforMap (abbreviated to SfM). To ensure a wide applicability, SfM is specifically designed to be applied on 110 a scale of 1 - 1000 km². The main objectives of this work are to:

- Present the SfM model as a tool for shallow landslide probability assessment.
- Show a calibration of SfM through a performance indicator over three study areas with 78 field recorded shallow landslide events in Switzerland
- Provide a qualitative sensitivity analysis and identify the parameters that are of greatest influence on the slope stability 115 of a given area.

Moreover, strong emphasis within the SfM framework and this paper is put on the quantification of root reinforcement on a regional scale. We will show the influence that an accurate representation of root reinforcement has on slope stability over the three study areas.



2 Methods: SlideforMap

120 2.1 Probabilistic modelling concept

SfM is a probabilistic model that generates a spatial distribution of shallow landslide probability (p_{SL}). It is an extension of the approach of Schwarz et al. (2010) and Schwarz et al. (2015). It generates a large number of hypothetical landslides (HLs, singular: HL) within the limits of a pre-defined region of interest. These HLs are assumed to have an elliptic shape and are characterized by a mix of deterministic and probabilistic parameters, based on which the landslide stability is computed following the limit equilibrium approach (see 2.2). The probabilistic parameters are the HL location, its surface area and its soil cohesion, internal friction angle and soil depth parameters (drawn from appropriate random distributions); the deterministic parameters include several vegetation parameters and hydrological soil parameters. A key originality of the approach stems from the fact that the vegetation parameters are derived from single-tree scale information (see 2.5). The number of generated landslides is selected high enough such that each point in a region of interest is overlain by multiple HLs from which a relative p_{SL} can be estimated by considering the ratio of unstable HLs. A general flow chart of SfM is given in Fig. 1. More details on the modules follow in the subsequent sections.

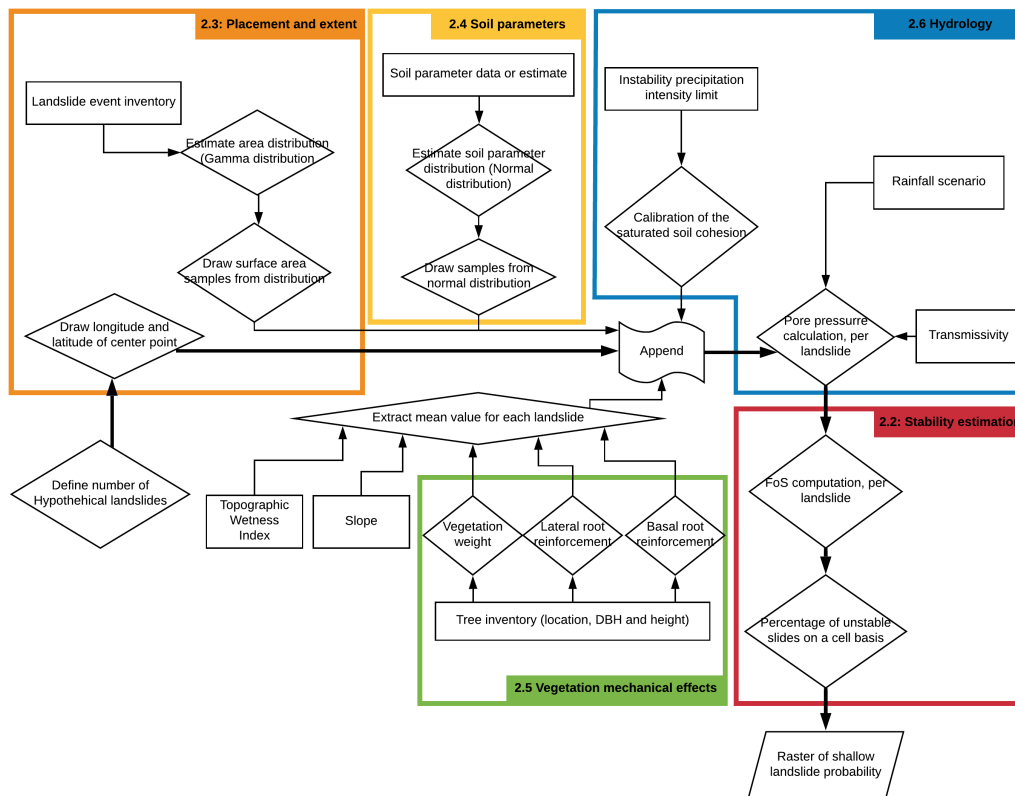


Figure 1. Flowchart of the computational steps in SfM. Separate sections are outlined in colors.



2.2 Stability estimation

The estimate of the stability of each HL is calculated following the limit equilibrium approach (described in the work of Day (1997)). In this method, a landslide is assumed to be stable if its safety factor (SF) is less than 1.0. The SF is computed as the ratio of the perpendicular (stabilizing) forces and the parallel (destabilizing) forces:

$$SF := \frac{F_{res}}{F_{par}} \quad (1)$$

where F_{par} [N] is the force parallel to the slope, F_{res} [N] is the maximum mobilized resistance force. The assumed forces that act upon a hypothetical landslide are schematically shown in Fig. 2.

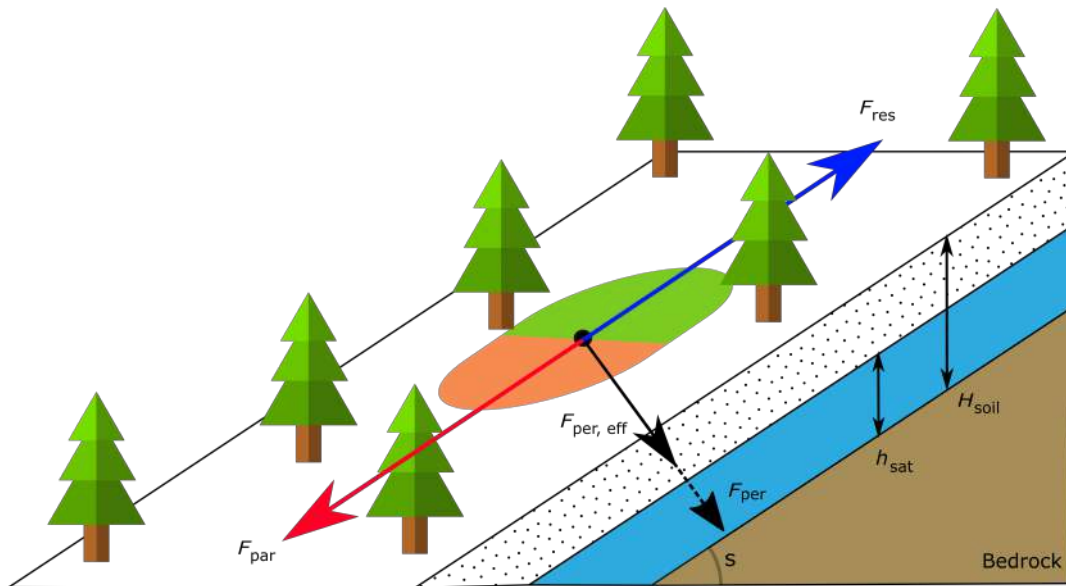


Figure 2. Schematic overview of the forces acting upon a hypothetical landslide, as assumed in SfM. Blue indicates the stabilizing forces and red indicates the destabilizing forces. Lateral root reinforcement only acts upon the green part of the hypothetical landslide. Whereas, basal root reinforcement and soil shear strength act on the whole potential failure surface.

As seen in Fig. 2, all landslides are assumed to be elliptical (Rickli and Graf, 2009) with a ratio between length and width, $l_{wr} = 2$. Quantification of the forces in the safety factor calculation follows the limit equilibrium assumptions. This method is outlined in equation 2 to 5 below:

$$F_{par} = g(m_{soil} + m_w + m_{veg}) \sin(s) \quad (2)$$

$$F_{res} = \frac{c_{ls}}{2} R_{lat} + F_{res,bas} \quad (3)$$



$$F_{\text{res,bas}} = A_{1s}C_{\text{soil}} + A_{1s}R_{\text{bas}} + F_{\text{per,eff}}\tan(\phi) \quad (4)$$

$$145 \quad F_{\text{per,eff}} = g(m_{\text{soil}} + m_w + m_{\text{veg}})\cos(s) - P_{\text{water}} \quad (5)$$

In these equations, m_{soil} is the soil mass [kg], m_w is the mass of the groundwater [kg], m_{veg} is the vegetation mass [kg], g is the gravitational acceleration assumed at $9.81 \text{ [m/s}^2\text{]}$, s is the slope [$^\circ$], c_{1s} is the circumference of the landslide [m], R_{lateral} is the lateral root reinforcement [N/m], $F_{\text{res,bas}}$ is the basal resisting force, A_{1s} is the area of the landslide, C_{soil} is the soil cohesion [Pa], R_{basal} is the basal root cohesion [Pa], $F_{\text{per,eff}}$ is the effective perpendicular resisting forces [N], ϕ is the angle of internal
150 friction [$^\circ$] and P_{water} is the water pressure [Pa].

2.3 Random landslide placement and extent

The location of the center of mass of the HLs is generated from two uniform distributions covering the latitudinal and longitudinal extent of the study area. HLs on the edge of the study area are taken into account as well, though cut to the extent of the study area in the later spatial processes of SfM. The total number of HLs is determined by multiplying the landslide density
155 parameter (ρ_{1s}) with the total surface area of the study area. This number is then uniformly sampled with replacements from the latitudinal and longitudinal distribution. The ρ_{1s} should be high enough such that each raster cell of the study domain is covered by several HLs. The HL surface area is sampled from an inverse gamma distribution, following the work of Malamud et al. (2004), which showed that the probability distribution of shallow landslide surface areas follows an inverse gamma distribution (Johnson and Kotz, 1970). The used parameterization of a three parameter inverse gamma distribution is shown in equation 6.

$$160 \quad P_A = \frac{1}{a\Gamma(b)} \left(\frac{a}{A_{1s} - c} \right)^{(b+1)} e^{-\left(\frac{a}{A_{1s} - c}\right)}, \quad (6)$$

where A_{1s} is the landslide surface area, P_A is the probability of A , Γ is the gamma function, a , b and c are the scale, shape and location parameters. These distributional parameters are estimated using the landslide surface area data of the inventory (section 3). The estimation is based on minimizing the Root Mean Square Error (RMSE) between the histogram counts (distance of 10) of the surface areas from the inventory and the distribution of equation 6. The maximum HL surface area is set for all case
165 studies based on the maximum surface area observed in the landslide inventory. This maximum is set to 3000 m^2 , based on the rounded up maximum value of a well-distributed landslide inventory in Switzerland (section 3.3).

2.4 Soil parameters

Steep-sloped mountainous areas are prone to extreme heterogeneity in soil parameters (Cohen et al., 2009). This makes a spatially deterministic parameterization inaccurate, even if based on observations. To overcome this limitation, a probabilistic



170 approach in the parameterization of the model is applied. Values of soil cohesion and internal friction angle of each HL are
randomly generated using independent normal probability distributions. The mean and a standard deviation of the distributions
may be defined based on different information such as field soil classification or a geotechnical analysis. Only positive gener-
ated values are retained, which leads to a non-Gaussian parameter distribution. This is critical in case of low mean values
and high standard deviations, which are however rare; truncating the distribution has thus little effect on the model results. The
175 soil cohesion in our computations is assumed to be representative for saturated, drained and unconsolidated conditions. Values
for soil depth are generated following a slightly different approach to account for the shallow soils found on steep slopes.
A random soil depth for each HL is obtained by first sampling h_{soil} from a normal distribution with mean m_d and standard
deviation σ_d , both derived from the observed soil depth distribution in the landslide inventory. This h_{soil} is then transformed as
a function of slope inclination:

$$180 \quad H_{\text{soil}} = h_{\text{soil}}(1 - P_{\mathcal{N}}(S \leq s | \mu_1, \sigma_1)), \quad (7)$$

where H_{soil} [m] is the soil depth and s is the observed slope, extracted for the HL. $P_{\mathcal{N}}(S \leq s | \mu_1, \sigma_1)$ is the cumulative normal
distribution of the slope S with $\mu_1 = 1.35 \cdot m_h$ and $\sigma_1 = 0.75 \cdot \sigma_h$. m_h and σ_h are the assumed mean and assumed standard
deviation of the slope angle of shallow landslides from an inventory or a best guess.

2.5 Mechanical effects of vegetation

185 Three properties of vegetation are included in the model. These are vegetation weight, lateral root reinforcement and basal root
reinforcement. Single tree detection ((Korpela et al., 2007; Menk et al., 2017)) serves as a basis to estimate these properties.
Single tree position and dimensions are derived from a Canopy Height Model (CHM), which is the difference between the
Digital Surface Model (DSM) and the Digital Elevation Model (DEM), using a local maxima detection method (LMD) de-
scribed in the work of Eysn et al. (2015) and Menk et al. (2017). First, the trees are rasterized. The resolution of this raster has
190 to exceed the effective radial dimension of the trees, in order to calculate representative vegetation parameter values at stand
scale. The weight of the tree is calculated by using the tree height and the Diameter at Breast Height (DBH), assuming that
the trees are cone shaped. The tree mass, m_{veg} , used in equation 2 and 5, is calculated assuming a mean tree density (ρ_{tree}) of
850 kg/m³. Root reinforcement is added in the model using the method proposed by Schwarz et al. (2015), which relates the
root reinforcement to the distance to a tree, the size of the tree and the tree species. The mean maximum distance of separation
195 (D_{trees}) of any point within a raster cell from a tree is given by equation 8 below. This equation considers a circular approach
to compute the mean maximum distance between trees:

$$D_{\text{trees}} = \sqrt{\frac{D_t^2}{\pi \cdot N_{\text{trees}}}}, \quad (8)$$

where D_t is the raster resolution used for the tree distance computation and N_{trees} is the number of trees per cell. The circular
approach follows multiple steps. First, we define a raster cell resolution for tree distance computation that is i) higher than the



200 underlying SfM raster resolution and ii) high enough such that each cell contains approximately the same number of trees. but
 not too large to prevent oversimplifying the forest structure. In SfM, 15 m is the default setting for this resolution. Subsequently,
 the surface area of this raster cell is divided by the number of trees in the cell (N_{trees}), providing the average surface area of a
 single tree in the cell. In conclusion, it is assumed that this area is occupied by the root system of a tree and that the radius of
 this tree area is the mean maximum distance (D_{trees}). This procedure is visualized in Fig. S-1 in the supplementary material.
 205 The lateral root reinforcement, R_{lat} , is then computed assuming that it is a function of the ratio of D_{trees} and DBH (Moos
 et al., 2016):

$$R_{\text{lat}} = c \cdot \Gamma \left(\frac{D_{\text{trees}}}{DBH \cdot D_{\text{trees,max}}} \middle| \alpha_1, \beta_1 \right), \quad (9)$$

where c is a fitting parameter, $\Gamma(x|\alpha_1, \beta_1)$ is the gamma density function evaluated at x with shape parameter α_1 and scale
 parameter β_1 . D_{trees} is the mean maximum distance to trees and DBH is the DBH. $D_{\text{trees,max}}$ is the coefficient between the
 210 DBH of a tree and the distance from the tree stem (Gehring et al., 2019), This is set to $D_{\text{trees,max}} = 18.5$ based on the work
 of Schwarz et al. (2010). The parameters of the gamma density function should be selected such that the function has a strictly
 decreasing behavior to avoid that R_{lat} increases with D_{trees} . These parameters should ideally reflect any knowledge about the
 how root reinforcement decreases with distance for specific tree species. Basal root reinforcement is assumed to be proportional
 to lateral root reinforcement and dependent on soil depth according to the relation shown in equation 10:

$$215 \quad R_{\text{bas}} = R_{\text{lat}} \Gamma(H_{\text{soil}}|\alpha_2, \beta_2), \quad (10)$$

where $\Gamma(x|\alpha_2, \beta_2)$ is the gamma density function evaluated at x with shape parameter α_2 and scale parameter β_2 . The param-
 eters α_2 and β_2 should be selected such that the function is decreasing with increasing H_{soil} .

2.6 Hydrology

Required hydrological parameters for the model are obtained based on a customized TOPMODEL approach (Beven and
 220 Kirkby, 1979; O'Loughlin, 1986; Montgomery and Dietrich, 1994). This method assumes macropore flow domination in
 hillslope hydrology. It is assumed that the saturated soil fraction of each cell holds a relation to its specific catchment area, its
 slope angle, a constant precipitation intensity and the soil transmissivity. In SfM, this relationship is parameterized following
 the work of Montgomery and Dietrich (1994), which is in close correspondence to the parameterization used in the widely
 used TOPMODEL (Beven and Kirkby, 1979):

$$225 \quad h_{\text{sat}}^* = \frac{P\theta}{T}, \quad (11)$$

where h_{sat}^* [-] is the fraction of saturation of a soil column, P [m/s] is the constant precipitation intensity, T [m^2/s] is the
 transmissivity and θ [m] is the topographic wetness index, TWI, in m^2 per meter contour length (see Section 3.2 for details)



on its computation). This index combines the specific catchment area and the slope angle. This approach uses the previously
discussed assumption (Section 1) that the drainage of intense rainfall is dominated by macropore flow, which has the ability to
230 quickly reach an equilibrium state with the precipitation input. In the subsequent computations, we assume that this equilibrium
state is reached in one hour. Using this estimated h_{sat}^* , pore water pressure is computed as:

$$P_{\text{water}} = H_{\text{soil}} \cdot \cos(s) \cdot h_{\text{sat}}^* \cdot g \cdot \rho_w, \quad (12)$$

where P_{water} [Pa] is the pore water pressure (used in equation 5), H_{soil} [m] is the soil depth, s is the slope angle, $g = 9.81 \text{ m/s}^2$
is the gravitational acceleration, ρ_{water} is the density of water assumed equal to 998 kg/m^3 . The same value for water density
235 is used in the computation of the water mass in the HL.

2.7 Model initialisation

The model has a total of 3 probabilistic parameters and 16 deterministic parameters (Table 1). The deterministic parameters
as well as the distributional parameters for the probabilistic parameters are determined from in-situ data or from literature (see
Section 3). In a first step of the workflow for the application of SfM, after assigning the deterministic parameter values and
240 sampling a value for each probabilistic parameter, a minimum value of soil cohesion is computed for each HL to obtain stable
conditions (safety factor, $\text{SF} \geq 1.0$) under a precipitation intensity of 28.3 mm/day . This threshold of precipitation intensity
is chosen according to (Leonarduzzi et al., 2017), who statistically analyzed 2000 landslides in Switzerland over the period
1972–2012 and found this as a triggering threshold. The minimum value of soil cohesion is obtained by equating F_{par} (equation
2) and F_{res} (equation 3). If the minimum value of soil cohesion is larger than the sampled soil cohesion, the soil cohesion is
245 updated to the minimum value.



Table 1. An overview of all model parameters of SfM. The last column indicates how the parameters are estimated (from data or literature)

Parameter	Description	Default value	Unit	Source
m_d, σ_d	Soil depth, mean and standard deviation	1, 0.25	m	Estimate
m_C, σ_C	Soil cohesion, mean and standard deviation	2, 0.5	kPa	Estimate
m_ϕ, σ_ϕ	Angle of internal friction, mean and standard deviation	30, 4	°	Estimate
ρ_{ls}	Density of the random generated landslides	0.1	HL/m ²	Estimate
ρ_{soil}	Dry soil density	1500	kg/m ³	Estimate
T	Soil transmissivity	0.1	m ² /s	Estimate
P	The precipitation event that is tested	10	m/s	Estimate
P_{min}	Precipitation intensity threshold for instability	1.2	m/s	Literature
D_t	Raster resolution for the tree distance computation	15	m	Estimate
r_{xy}	Raster resolution of the SlideforMap run	2	m	Estimate
l_{wr}	Ratio between length and width of the elliptical landslides	2	-	Estimate
c	Fitting parameter for the lateral root reinforcement	25068.54	-	Literature
α_1, β_1	Gamma function shape and scale parameter of the lateral root reinforcement	0.862, 3.225	-	Literature
$D_{trees,max}$	maximum distance for influence of tree roots	18.5	m	Literature
α_2, β_2	Gamma function shape and scale parameter of the basal root reinforcement	1.284, 3.688	-	Literature
ρ_{tree}	Density of a tree	850	kg/m ³	Estimate
ρ_{water}	Density of water	998	kg/m ³	Estimate

2.8 Landslide probability computation

After model initialisation, SF (equation 1) is computed for each of the generated HLs. Based on the SF for all generated HLs, landslide probability, p_{SL} , is computed as:

$$p_{SL} = \frac{n_{us}}{n_{HL}} \quad (13)$$

250 where n_{us} is the number of unstable HLs, i.e. of HLs with SF<1.0 and n_{HL} is the total number of generated HLs (the HLs are overlapping).



3 Data

3.1 Study areas

Three study areas were chosen to test SfM based on the availability of elevation data and detailed records on historical shallow
255 landslide events (Fig. 3), each varying in size and location to test the robustness and the general applicability of the model.

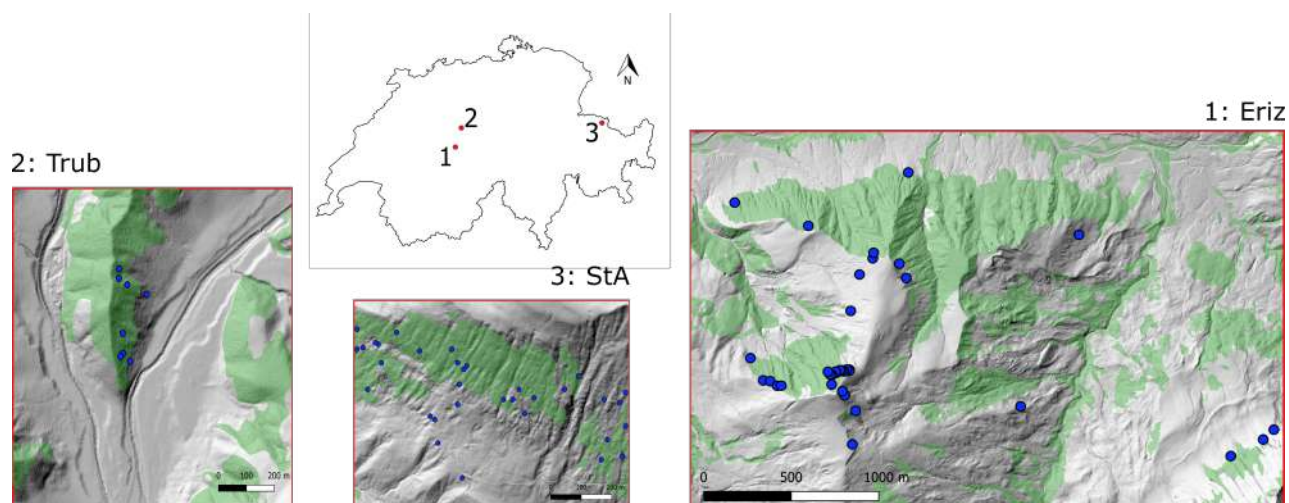


Figure 3. Locations of the study areas in Switzerland with observed Shallow landslide occurrence over the period 1997 - 2012 (blue dots); the case study names are given according to nearby villages: Trub, St. Antönien (short: StA) and Eriz. Forest covered area is presented in green (source: Swisstopo, 2020).

The geological formations in the Eriz study area vary from Oligocene freshwater Molasse in the lower northern part, morainic material in the central part and Cretaceous Limestone in the highest parts. Forests are dominated by spruce (*Picea abies*), except for the lower regions where broad-leaved trees are dominant. In the Trub study area, the dominant geological formation is Miocene Marine Molasse and forests are dominated by spruce. In the St. Antönien study area, the dominant geological
260 formation is Flysch (Prättigauer Flysch), partially covered by till (Moos et al., 2016). The forest in this study area is also dominated by spruce (Moos et al., 2016). Further characteristics of the study areas are given in Table 2.



Table 2. Study area characteristics. Meteorological data is from the HADES yearly average precipitation for the time period 1981 - 2010 (Frei et al., 2020).

Name	Centre coordinate lat;lon (WGS84)	Surface area km ²	Mean prec. mm/year	Elevation range m.a.s.l.	Inventoried slides	Mean slope °
Eriz	7.81; 46.78	7.54	1700	960 - 1750	37	20.4
Trub	7.90; 46.96	1.00	1620	820 - 1020	8	18.3
StA	9.80; 46.98	0.56	1310	1540 - 2010	33	27.5

3.2 Input data

To accurately measure p_{SL} for each study area, the following data are required.

- Digital Surface Model (DSM) and Digital Elevation Model (DEM)
- 265 – Average and standard deviation values for soil cohesion, depth and friction angle
- A representative landslide inventory containing at least:
 - Average landslide soil depth
 - Landslide surface area

In addition to the DEM, the DSM is applied in the vegetation section of SfM. The DEM and the DSM are both acquired from
 270 the SwissAlti3D database (Swisstopo, 2018), which makes use of aerial laserscanning (ALS). Both the DSM and DEM are
 available at a resolution of 0.5 m. For the computation of the maximum distance from trees (equation 8), the DEM is (nearest
 neighbour) resampled to 15 m to ensure a stable computation, since a too high raster resolution would result in too strong
 differences between raster cells with trees and raster cells without trees. After pit filling, the DEM is used to compute a slope
 map following the method of Zevenbergen and Thorne (1987). The topographic wetness index θ for equation 11 is computed
 275 on a raster cell basis based on the 2 m DEM using equation 14:

$$\theta = \frac{A_{cat}}{\sin(s)}, \quad (14)$$

where A_{cat} is the specific upslope catchment area and s is the slope angle. To avoid numerical problems for elongated catch-
 ments, θ is computed using a 2 km buffer around the catchment. The standard D8 method is applied for the computation of
 the upslope catchment area from the DEM (O’Callaghan, J and Mark, D, 1984). For single tree detection, the FINT algorithm
 280 (Menk et al., 2017) is used. Since the results of such detection methods are strongly influenced by the resolution and smooth-
 ness of the input data (Eysn et al., 2015), we applied the local maxima detection method, LMD, to the a canopy height model
 (CHM). This canopy height model is computed by subtracting the DEM from the DSM and is resampled to a resolution of 1,



1.5 and 2 m. In addition, three different Gaussian filters were applied on the 1 m resolution CHM. These three filters have a radius of 3, 5 and 7 cells and a standard deviation of 2 m. To identify the input data that leads to LMD results with the highest accuracy, we evaluated the identified trees in three randomly selected forest inventory plots with an area of 20 m x 20 m for each study site. In these plots, we visually identified all recognisable tree crowns, on the basis of aerial photos ((Swisstopo, 2017)) and the CHM. The identified trees were then compared to the LMD result, using the difference in the number of detected trees. The input data leading to the most accurate results in all three study sites was the 1 m resolution CHM with a Gaussian filter of a 3 cells radius and with the fixed standard deviation of 2 m. This combination has been applied to the entire area of the three study sites. To estimate the diameter at breast height (DBH) from the tree heights of all detected trees, the following empirical equation (Dorren, 2017) was used:

$$DBH_{tree} = H_{tree}^{1.25} \quad (15)$$

where DBH_{tree} [m] is the diameter at breast height of a given tree and H_{tree} [m] its height. Details resulting from the LMD method for the three study areas are shown in Table 3.

Table 3. Vegetation parameters in the study areas. The forest cover is derived from Swisstopo (2020)

Study area	Trees identified	Forest cover %	Mean stem density Stems/ha	Mean DBH cm	Std. deviation DBH cm
Eriz	38923	32	165	51	27
Trub	7267	26	270	55	30
StA	1796	27	120	31	18

The lateral and the basal root reinforcement (equations 9 and 10) are parameterized using the values from Gehring et al. (2019) ($\alpha_1 = 0.862$, $\beta_1 = 3.225$, $c = 25068.54$, $\alpha_2 = 1.284$, $\beta_2 = 3.688$). In their work, the calibration was performed on beech (*Fagus Sylvatica*) stands over varying elevations. Our study areas, however, are predominantly vegetated by spruce trees. Therefore a discrepancy in the estimated root reinforcement will likely arise. Unfortunately, however, this is the only published set of calibrated values.

3.3 Landslide inventory

A landslide inventory is required to quantify a distribution for slope, surface area and soil depth for the HLs. This inventory does not necessarily have to be well distributed in the study area, or even be present in the area. However, it should be representative of the conditions in the area of interest as much as possible. A dataset of 668 landslides that occurred between 1997 and 2012 in Switzerland has been created by the Swiss Federal Office for the Environment (Rickli et al., 2019). Statistical information



305 on the landslides can be seen in Fig. 4. The landslides in the St. Antönien and Trub area took place in 2005 during or shortly after heavy rainfall in August. The landslides in the Eriz area from 2012 are related to heavy rainfall in July.

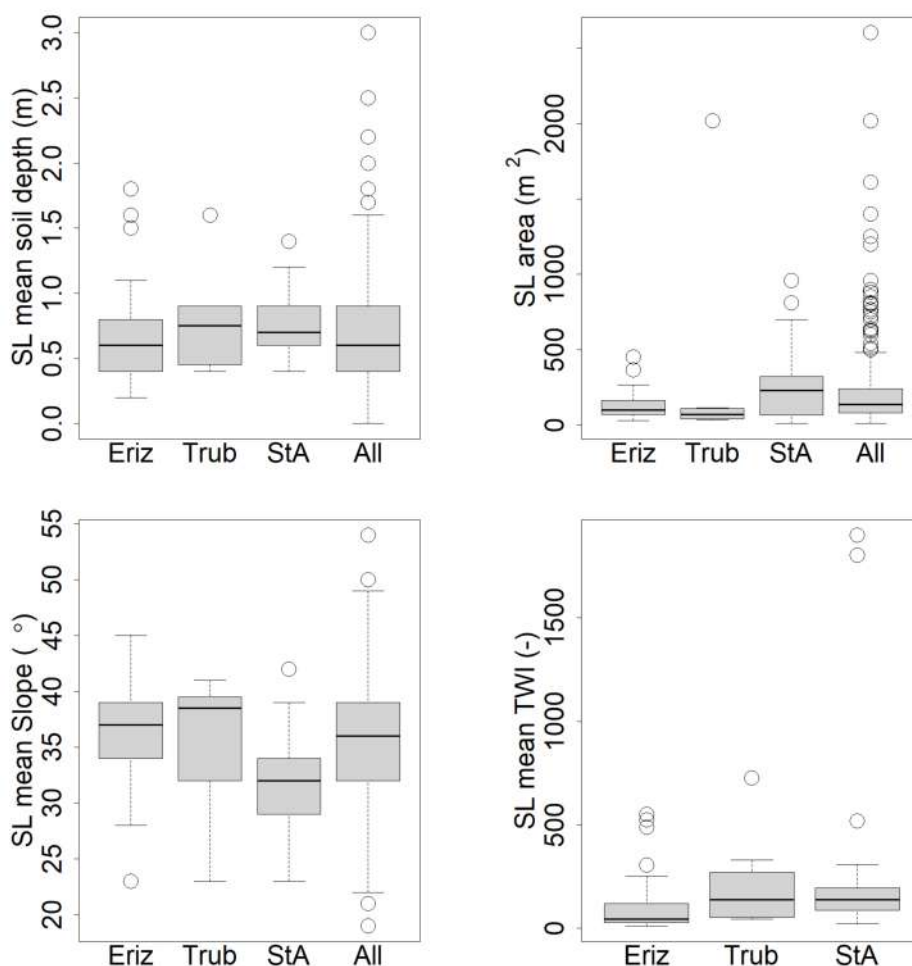


Figure 4. Overview of landslide properties for the studied regions. Top row: mean soil depth (left) and the surface area (right) of the shallow landslide (SL) for the test areas and the total inventory; bottom row: mean slope (left) and mean TWI (right). The box plots show the 25, 50 and 75 percentiles, the whiskers extend to 1.5 times the length between the 25 and 75 percentile. Outliers are marked as circles. The TWI was extracted from the TWI raster cells that lie inside the landslide inventory polygons.

The inventory is used to estimate the parameters for the surface area distribution used in SfM (equation 6), via minimization of the RMSE between observed frequencies and theoretical frequencies. The estimated values of the slope, scale and location parameters are: $a = 1.40$, $b = 1.5^{-4}$, $c = 4.28^{-8}$.



310 3.4 Model calibration and sensitivity analysis

The model has a total of 22 parameters that are derived from observed data, from literature or that are set to default values; their values, given in Table 1, are not further varied in the model behavior analysis. These parameters are: P_{\min} , D_t , l_{wr} , c , α_1 , β_1 , $D_{\text{trees,max}}$, α_2 , β_2 , ρ_{tree} , ρ_{water} . The remaining parameters are then calibrated by Monte Carlo simulation, drawing a high number of parameter samples for all calibration parameters and evaluating the corresponding model performance based on the Area Under the Curve (AUC) method (Metz, 1978; Fawcett, 2006). We hereafter first present the used performance evaluation method, followed by the parameter sampling method used for the calibration as well as for the sensitivity analysis. In addition, we present four vegetation parameter scenarios that are developed to test the potential influence of vegetation.

3.4.1 Model performance evaluation

The basis of the application of the AUC method is a spatial representation of the landslide inventory in a boolean raster (0 = no past landslide present, 1 = past landslide present). For each randomly generated parameter set, the simulated $p_{\text{SL}} 2.8$ is also converted to a boolean raster, by selecting a threshold to assign 0 or 1. Overlaying the inventory raster on the modelled raster, results in a confusion matrix with four possible combinations, as shown in Table 4.

Table 4. The confusion matrix, as used in the calibration.

		Model	
		True	False
Inventory	True	True positive (TP)	False negative (FN)
	False	False positive (FP)	True negative (TN)

For every threshold value, the sensitivity, $TP/(TP+FN)$, and the specificity, $TN/(TN+FP)$ are computed. Plotting the sensitivity and specificity against each other for all thresholds results in a Receiver Operator Curve (ROC). The area under the ROC curve is the AUC and defines the accuracy of the model on a scale of 0.5 - 1.0, where 0.5 is being no better than a random guess and 1.0 is a perfect prediction.

3.4.2 Parameter sampling and qualitative sensitivity

The parameter samples for the Monte Carlo-based model calibration and the subsequent sensitivity analysis are generated using the Latin Hypercube Sampling (LHS) technique (McKay et al., 1979). This makes use of semi-random samples of variables over pre-defined ranges. The outcome of a Monte Carlo-based calibration is highly influenced by the ranges chosen for the parameters. For this reason, parameter ranges were chosen as realistically as possible. To estimate the parameter ranges for soil properties, soil types in USCS classes are taken from the shallow landslide inventory ($n = 377$). Soil types present more than ten times are taken into account and aggregated into a hybrid Table of soil cohesion and angle of internal friction values



per soil type based on the values given in the work of Dysli and Rybisar (1992) and VSS-Kommission (1998) (see Appendix,
 335 Table A1).

To obtain a range for parameter sampling via LHS, first the weighted mean soil cohesion is computed from the soil types
 and then the weighted standard deviation is subtracted and added twice to the weighted mean. This is to account for 95% of
 the variation in the observed soil cohesion (assuming a normal distribution). The same procedure is performed for the angle of
 internal friction. The range of transmissivity values is obtained by taking the saturated hydraulic conductivity from the work
 340 of Freeze and Cherry (1979) for the respective soil classes and by multiplying these saturated hydraulic conductivities with the
 minimum and maximum soil depth of the soil class. From the resulting list of possible transmissivity values per soil class, the
 minimum and maximum are taken for the LHS range. The precipitation intensity range is defined by the lowest 1 hour intensity
 corresponding to a return period of 10 years and the highest 1 hour intensity corresponding to a return period of 100 years over
 the study areas. These are computed using data from the work of Jensen et al. (1997) and the methodology as described in the
 345 work of HADES (2020). The maximum value for vegetation weight is taken from a biomass study in Switzerland by Price et al.
 (2017). For the other parameters, realistic ranges have been assumed. In Table 5 an overview is given of the tested parameters
 and the ranges used to generate the parameter samples.

Table 5. Parameters used in the SfM qualitative sensitivity analysis and corresponding ranges for parameter sampling via LHS.

Parameter	Unit	Description	LHS Range
ρ_{ls}	m^{-2}	Density of the randomly generated landslides	0.02 - 0.10
ρ_{soil}	kg/m^3	Dry soil density	1.00 - 1.50
m_d	m	Mean soil depth	0.20 - 1.80
σ_d	m	Standard deviation of the soil depth, as a fraction of m_d	0.00 - 0.50
m_C	kPa	Mean saturated soil cohesion	0.00 - 12.5
σ_C	kPa	Standard deviation of the soil cohesion, as a fraction of m_C	0.00 - 0.50
m_ϕ	°	Mean angle of internal friction	24.00 - 41.50
σ_ϕ	°	Standard deviation of the angle of internal friction	0.00 - 5.00
T	m^2/s	Soil transmissivity	10^{-8} - 10^{-3}
P	mm/h	The precipitation event that is tested	32.0 - 50.0
R_{lat}	kPa	Assumed lateral root cohesion	0.00 - 15.0
W_{veg}	tonne/m ²	The weight of the vegetation	0.00 - 0.10

For the model calibration and qualitative sensitivity analysis, 1000 LHS parameter sets were generated per study area. For all
 corresponding SfM model runs, vegetation is set to a global uniform vegetation, which results in constant root reinforcement
 350 and vegetation weight in space. This is necessary because the same runs are used for model calibration and for model sensitivity
 analysis, where we need such uniform vegetation to ensure that the sensitivity of the (hypothetical) vegetation has an effect



on all raster cells of the whole study area (and not only on the actually vegetated cells). The parameter set with the highest AUC value is retained for model calibration. In addition, all 1000 parameter sets are used for a qualitative sensitivity analysis. The influence of each individual parameter on a response variable is observed by filtering the runs on best performance. The response variables are the AUC as a measure for accuracy and the ratio of unstable landslides as a measure for instability.

3.4.3 Vegetation parameter scenario analysis

SfM has potential in testing the effect of different vegetation scenarios on the landslide probability. For this research, besides the reference scenario for model calibration and sensitivity analysis (global uniform vegetation), three additional scenarios are tested: i) without vegetation, ii) with uniform vegetation in forested areas and iii) with a fully diverse vegetation based on single-tree detection. The forested areas are defined as areas where the single tree detection method leads to a lateral root reinforcement (Fig. 9) which is not equal to zero.

4 Results

All the results presented hereafter are based on a ρ_{ls} of $0.1 \text{ HLLs}/\text{m}^2$ per model run.

4.1 Model calibration

Based on the generated 1000 parameter sets, we identified the parameter set that resulted in the highest AUC value and assumed this to be an optimal calibration of the model. These calibrated parameter sets for each study area and their AUC values are shown in Table 6 together with the ratio of generated HLs that are unstable.

Table 6. Outcome of the Monte Carlo-based calibration: the parameter sets per study area resulting in the highest AUC value. The last row shows the ratio of unstable HL resulting from these parameter sets.

Parameter	Eriz	Trub	StA	Parameter	Eriz	Trub	StA
ρ_{ls}	0.096	0.092	0.064	σ_{ϕ}	3.01	3.18	1.41
ρ_{soil}	1.45	1.45	1.37	T	0.000437	0.000910	0.000949
m_d	1.28	1.24	1.75	P	45.4	35.3	35.7
σ_d	0.15	0.11	0.16	R_{lat}	3.17	8.23	1.75
m_C	4.91	1.11	3.71	W_{veg}	0.05	0.09	0.07
σ_C	0.21	0.16	0.42	AUC	0.916	0.935	0.686
m_{ϕ}	39.90	41.4	25.69	Unstable Ratio.	0.126	0.148	0.708

Most of the calibrated parameter values display relatively similar values across all case studies, with a maximum difference between the case studies that is smaller than half of the LHS range. The exceptions to this are the standard deviation of the soil



370 cohesion, σ_C , the mean angle of internal friction, m_ϕ , the transmissivity T and the precipitation intensity, P , with m_ϕ showing
the strongest variation between case studies. Overall, this suggests that the calibration is robust for these regions. The shallow
landslide probability computed with SfM for the three areas with their calibrated parameter set is given in Fig. 5.

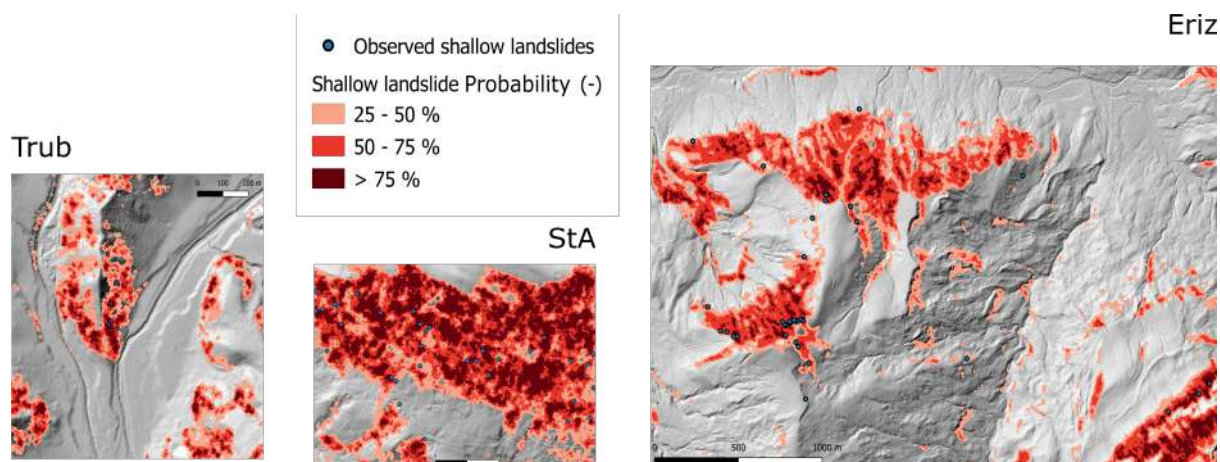


Figure 5. Overview of the landslide probability of the study areas simulated with the calibrated parameter sets of Table 6. Added as blue points are the observed landslides from the inventory.

The model represents well the spatial distribution of the shallow landslides from the inventory. The simulated shallow landslide probability patterns show a strong difference in the ratio of unstable HLs (Table 6) between the StA and the other study areas,
375 as shown in Fig. 5 and further emphasized in Fig. 6, which shows a strong difference of the cumulative density of landslide probability between the StA study area and the two other areas.

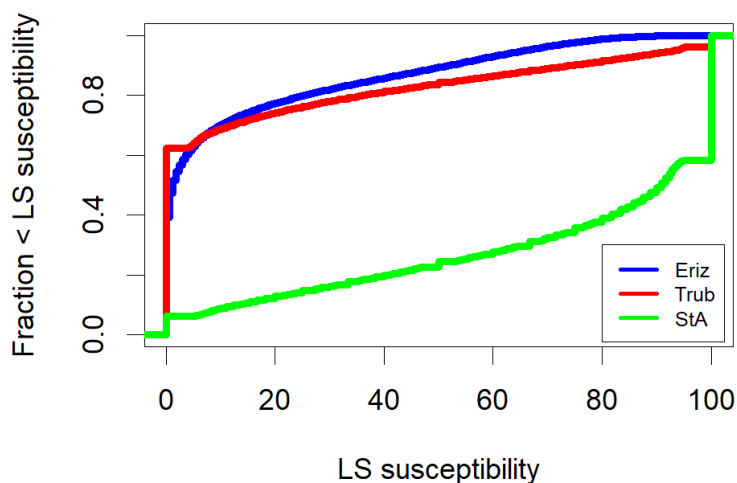


Figure 6. Cumulative plots for shallow landslide probability in the study areas, derived from the results in Fig. 5.

4.2 Sensitivity analysis

The 1000 parameter sets per study area were used for qualitative sensitivity analysis where we analyzed how the parameter distributions changed if we retained only a subset of parameters, as a function of their AUC values or of their landslide probability.
380 The effect of subsampling was analyzed based on the empirical parameter distributions (i.e. histograms) of each parameter, which represents their empirical marginal distribution (i.e. the distribution of one parameter given all other parameter distributions).

For some parameters, the histogram shape (i.e. their marginal distribution) does not significantly deviate from a uniform distribution, even if we retain only the best 10% (in terms of AUC) of all parameter sets (Fig. 7). This apparent lack of
385 sensitivity does not necessarily mean that the model is not sensitive to this parameter; in fact, the sensitivity could be hidden by strong parameter correlation (see Bárdossy, 2007, for a discussion of how uniform marginal distributions can result from strong parameter correlation). Some parameters, in exchange, show very strong sensitivity of their marginal distributions if only the best (in terms of AUC) parameter sets are retained. For the Trub case study (Fig. 7), we see that the mean depth m_d , the mean cohesion m_c and the transmissivity T show a well defined maximum around the parameter values retained for calibration (the
390 best performing ones. This suggests a good sensitivity of the model to these three parameters in terms of model performance. Two of these three parameters also show a clear sensitivity if we retain subsamples that lead to successively higher unstable landslide ratio (Fig. 8): high unstable ratios are obtained for high m_d values or for low m_c . Also for R_{lat} , highest ratios are clearly obtained for low lateral root reinforcement values (for all three case studies, Fig. 8, Supplementary Material S-3, S-5).



395 For transmissivity, while it shows a clear effect on model performance, there is no clearly visible relation between its marginal
distribution and the ratio of unstable landslides.

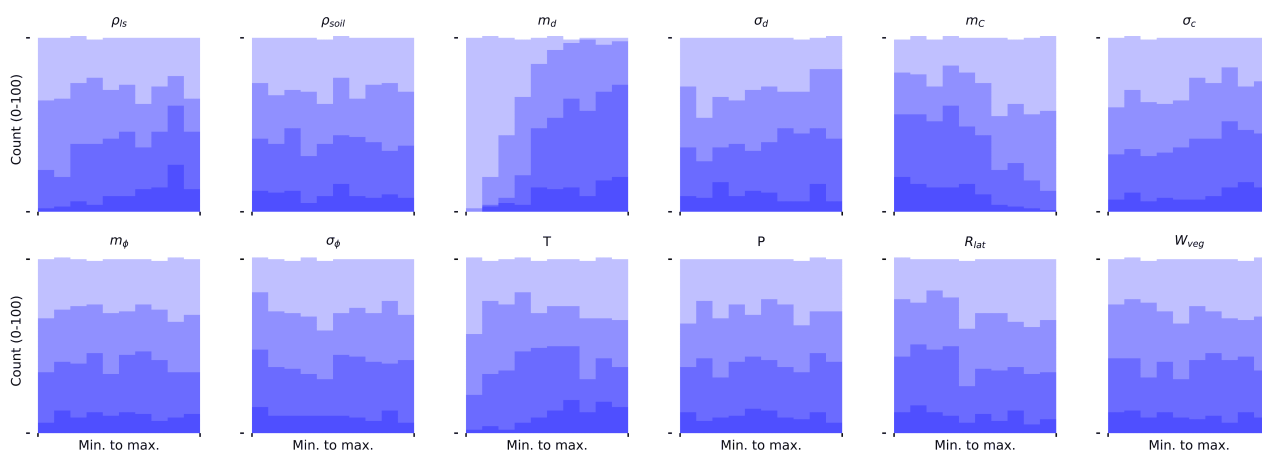


Figure 7. Histograms of different subsamples of the LHS parameter sets for the Trub study area. The shading (from light to dark) corresponds to subsamples retaining only the $x\%$ best parameter sets in terms of AUC; the shown fractions are: 1, 0.7, 0.4, 0.1.

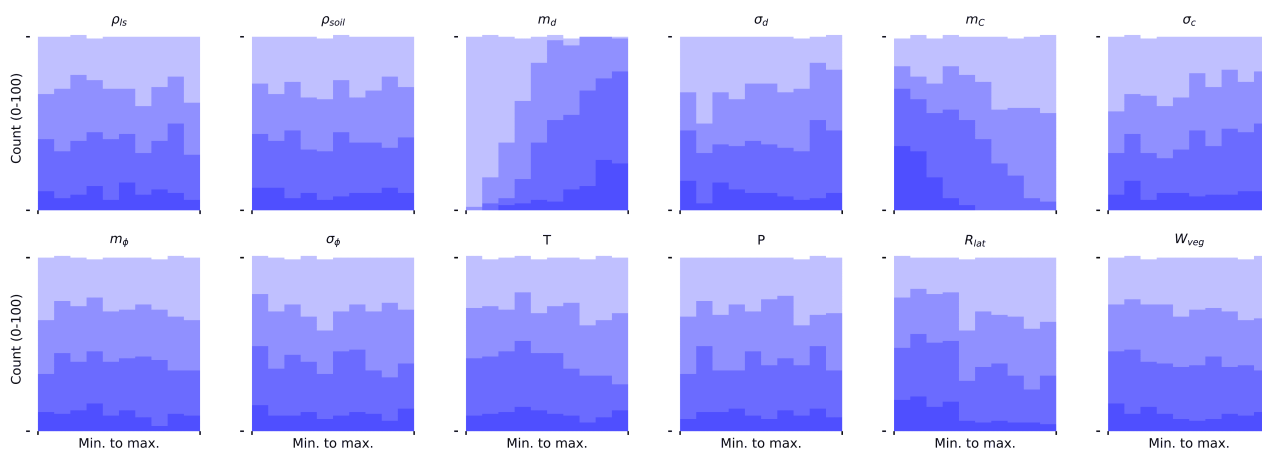


Figure 8. Histograms of different subsamples of the LHS parameter sets for the Trub study area. The shading (from light to dark) corresponds to subsamples retaining only the $x\%$ best parameter sets in terms of Unstable ratio; the shown fractions are: 1, 0.7, 0.4, 0.1.

4.3 Mechanical effects of vegetation

To test the impact of vegetation on the model behavior, we compare the different vegetation scenarios. The spatial distribution of lateral root reinforcement, resulting from single tree detection and SfM, is given in Fig. 9.

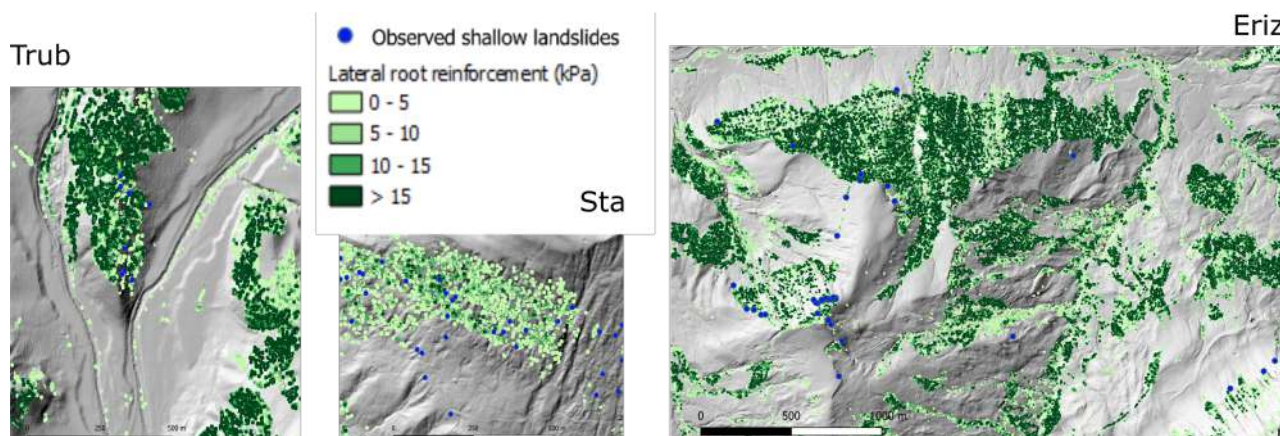


Figure 9. The spatial distribution of root reinforcement in the study areas as used in SfM.

The selected vegetation scenarios (no vegetation, global uniform vegetation, forest area uniform vegetation, single tree detection) affect the computation of the vegetation weight, of the lateral root reinforcement and of the basal root reinforcement. The latter is due to its dependence on lateral root reinforcement (equation 10). Accordingly, the vegetation scenario has a direct impact on SF (equation 1, 3, 4) and on p_{SL} (equation 13). For the analysis, we use the optimal parameter set from Table 6, obtained for a global uniform vegetation cover. The model runs are repeated 10 times to produce an average result and to show the variation from the probabilistic approach. The resulting influence of the selected vegetation scenarios on AUC and ratio of unstable landslides is given in Table 7.

The results show that compared to the reference scenario used for calibration, the AUC remains almost unchanged or slightly increases for the vegetation based on single tree detection. In exchange, the ratio of unstable landslides significantly decreases for all case studies with single tree detection and significantly increases without vegetation. This result clearly shows that the model shows a good sensitivity to the vegetation scenarios and that it correctly predicts lower ratios of unstable fractions for single tree detection, which corresponds to the assumed stabilizing effect of the realistic vegetation cover compared to a uniform vegetation cover. This underlines the value of the model for future for scenario analyses. The model performance, in exchange, is not sensitive enough to decide during model calibration, which vegetation scenario is more likely for a given case study. While not being critical for scenario analysis, this problem could be related to the amount of reference data and could be overcome by redesigning a new performance criterion that accounts explicitly for a potential lack of reference data.



Table 7. AUC and unstable ratio under different vegetation scenarios with the optimal parameter sets of Table 6 and averaged over 10 runs. The "Overall" is composed of the mean value of all three study areas. In the global uniform vegetation scenario, the reference scenario is used during parameter optimisation.

		AUC				Unstable ratio			
		Overall	Eriz	Trub	Sta	Overall	Eriz	Trub	Sta
mean	Global uniform vegetation	0.825	0.908	0.920	0.647	0.326	0.126	0.147	0.704
	Forest area uniform vegetation	0.826	0.904	0.920	0.653	0.326	0.127	0.147	0.705
	Single tree detection	0.843	0.906	0.955	0.669	0.293	0.071	0.120	0.688
	No vegetation	0.825	0.908	0.920	0.648	0.394	0.167	0.276	0.740
Std. dev.	Global uniform vegetation	0.005	0.006	0.004	0.006	0.001	0.001	0.001	0.002
	Forest area uniform vegetation	0.009	0.008	0.004	0.014	0.001	0.000	0.001	0.002
	Single tree detection	0.009	0.011	0.003	0.012	0.001	0.000	0.001	0.001
	No vegetation	0.008	0.008	0.004	0.011	0.001	0.000	0.001	0.00

415 5 Discussion

It is important to point out that the inventory to which the model performance is calibrated plays a key role in all the results discussed below. The inventory was obtained after a single rainfall event, for which the precipitation intensity, duration and the spatial distribution are not known exactly. Despite of this, the inventory represents a unique source of information and the spatial localisation of the landslides can be assumed to be of high quality. Below, we discuss the model behavior as a function
 420 of the different model parameter groups, discuss the performance of the model and give directions for future research.

5.1 Soil parameters

The best performing parameter sets show coherently high values for the soil depth for all study areas (by comparing the values of Table 6 and Table 5). The qualitative sensitivity analysis (Fig. 8) also shows that the highest unstable ratios are obtained for highest soil depths; this indicates that a certain minimum soil depth is required for landslide triggering, which is in line
 425 with previous findings by D’Odorico and Fagherazzi (2003) and by Iida (1999). In these studies, soil depth is noted as the conditional factor for landslide triggering along with precipitation intensity and duration. The best performing parameter sets display a certain variation for the mean cohesion across the three case studies (Table 6), with a clear tendency to low values in all study areas (Fig. 8, Supplementary Material S-5, S-3), which suggests that the observed landslides can only be reproduced with low soil cohesion for all case studies. The mean angle of internal friction shows a high variation, from a very low value
 430 for StA to close to the maximum tested value for Trub (which suggests that even higher values could be tested in the future). This might be attributed to the difference in geology and soils between the study areas.



5.2 Hydrological parameters

Soil transmissivity showed considerable sensitivity to the AUC (Fig. 7) and the values are consistently high for all three case studies for the test LHS range (Fig. 6), which is a hint that a correct estimation of soil transmissivity is paramount for a reliable estimate of shallow landslide occurrence. Regarding precipitation intensity, we see a certain variability between the best values for the three case studies and no clear univariate sensitivity of the model performance or the model output (ratio of unstable landslides). It is notable, however, that calibrated conditions in all study areas resulted in a majority of HLs being in fully saturated soil conditions. The application of the TOPMODEL approach has the major shortcoming that it assumes a groundwater gradient parallel to the surface gradient. It has been shown in the past that this assumption decreases the accuracy of water content simulations as compared to distributed dynamic hydrological models (Grabs et al., 2009). However, as discussed earlier, it has also been shown in the past that macropore flow is omnipresent in landslide triggering and SfM has been parameterized assuming an important role of macropore flow. In macropore-driven systems, steady state groundwater flow is easily reached (section 1), which implies that the TOPMODEL assumption holds well in this case. In the landslide inventory underlying the study here, the dominant soil types are GM (silty gravel), GC (clayey gravel) and CL (low plasticity clayey silt); accordingly, we can assume that the TOPMODEL assumptions are valid for a wide range of the domain (for GM and GC soil type), even if it holds probably less well for the CL soil types. In addition to the limitation related to TOPMODEL, SfM assumes rainfall to be constant both in space and time, which could however easily be relaxed in the future.

5.3 Vegetation

A key aspect of the presented model is the use of single tree detection to parameterize vegetation, a method that was previously found by Menk et al. (2017) to be reliable to detect single trees and derive their DBH's from the detected tree heights for sloped forests. As mentioned in Section 3.1, we found for the selected case studies that single tree detection provides the best results in terms of correct number of trees counted if applied on a 1 m resolution DSM with a 3 cell kernel Gaussian filter. This is in line with the results of Menk et al. (2017) who found in a similar scenario-testing approach that a 1 m resolution DSM with no Gaussian correction provided the most accurate results, noting, however, that the difference in performance between these two methods (with and without Gaussian filter) is small. In SfM, we are not only considering basal but also lateral root reinforcement. This is unique for shallow landslide probability models. As shown in the sensitivity analysis (Fig. 8), R_{lat} has a clear effect on the ratio of unstable landslides, with low values leading to high ratios. However, in the SfM workflow and calibration, a fixed relationship between the lateral and the basal root reinforcement is assumed, accordingly, the model sensitivity cannot be attributed to R_{lat} or R_{bas} . Mobilization of the lateral root reinforcement in the SfM workflow is independent of time and not countered by passive earth pressure. A shortcoming in this parameterization of the effect of vegetation is the assumption of uniform forest structure and a uniform tree species (beech) within a landslide area. The field recordings in the St. Antönien area of Moos et al. (2016) show that the forest consists mainly of Norway spruce. For the Trub and Eriz area, visual interpretation of aerial photos allowed us to identify mixed forests with Norway spruce and beech. The latter are known for having a high root reinforcement and therefore the beech assumption will overestimate both the lateral and



465 the basal root reinforcement (Gehring et al., 2019). Subsequently, vegetation weight shows no clear relation to both the AUC
and the unstable Ratio (Fig. 7, Fig. 8). However, this does not mean that vegetation weight does not influence the response
variables. The relationship could depend too strongly on other parameters to be directly visible (Bárdossy, 2007).

5.4 Implementation of the mechanical effects of vegetation

In Table 7 it can be seen that the vegetation scenario has a considerable impact on the modelled Unstable ratio for all study
470 areas. The decrease of the unstable ratio under the realistic (single-tree based) vegetation cover as compared to the uniform
vegetation cover, is, however, considerably smaller for StA than for the other two case studies. This is probably related to the
fact that overall, conditioned on the observations, the simulated unstable ratio is quite high and even any kind of vegetation
arrangement cannot significantly reduce this ratio. Our overall finding that the model output (ratio of unstable fraction) is
highly sensitivity to the vegetation scenario and gives lowest values for single-tree detection (realistic vegetation cover). This
475 is inline with the findings of Roering et al. (2003), who state that single tree based modelling, including the tree dimensions,
has by far the highest accuracy in the prediction of shallow landslides. Moreover, Vergani et al. (2014) state that a site specific
estimation of vegetation and root extent is essential in the correct estimation of root reinforcement.

5.5 Model performance

As pointed out by Corominas et al. (2014), the absolute values of AUC are dependent on the characteristics of the study area.
480 In larger areas, with low overall landslide activity, the AUC will overestimate the predictive performance. This most likely
explains why the StA study area has a low overall AUC compared to Eriz and Trub (Table 7). In particular, StA study area
shows a higher prevalence of steep slopes. The Trub and the Eriz study area show both relatively high AUC values, indicating
high model performance, which in addition are very similar AUC values; this is in agreement with a similar occurrence of
steep and gradual slopes in these areas. Another explanation for the discrepancy in model performance between the study areas
485 could be the assumption that all trees are beech trees. This does not hold equally well for all three study areas. Based on visual
inspection and on elevation, the mismatch between actual vegetation and this assumption is probably most pronounced in the
StA area, where the dominant tree species appears to be Spruce. Though no published data is available, it can be estimated
from the work of Moos et al. (2016) that the root reinforcement of a spruce forest is lower than that of a beech forest, which
can however, at this stage not be confirmed by our parameter analysis.

490 Finally, we would like to add here that the case study dependence of the used model performance measure is a limitation that
typically occurs for all model performance measures that compare the model behavior to some reference model (Schaeffli and
Gupta, 2007) (the reference model for AUC is a random process). Accordingly, we cannot compare the performance of SfM to
other published AUC values despite of the fact that values around 0.8 are generally considered as indicating good performance
(e.g. Xu et al., 2012).



495 5.6 Future research

SfM uses a relatively simple hydrological module to estimate soil saturation. The used classic TOPMODEL approach could be improved and multiple papers have presented simple to more advanced rewriting of the TOPMODEL formulas (e.g. Beven and Freer, 2001; Blazkova et al., 2002). Common denominator is the inclusion of time dependency, since the stationary flow assumption rarely, if ever, holds in nature. This time dependency is a solution to simulate a different response to a precipitation event at different locations within a study area. Future work could also focus on improving the vegetation module by including different tree species (those that are often used in protection forest) in the parametrization of lateral root reinforcement (equation 9).

6 Conclusions

In this paper, we present a probabilistic model to assess shallow landslide probability. The main motivation to develop yet another model is to provide a detailed inclusion of the influence of vegetation. The key elements of the model parameterization are the mean soil depth, the mean soil cohesion, the soil transmissivity and the lateral root reinforcement. Its application is illustrated based on three mid-elevation case studies from Switzerland, for which a detail landslide inventory is available. The model has a total of 22 parameters, of which 12 are calibrated using the AUC of the Receiver Operator Curve as performance measure to identify the best parameter set among a large set generated using Latin hyper cube sampling. The AUC maximum values for the three study areas vary between between 0.69 and 0.94 under a spatially uniform vegetation scenario, which reflects an overall good model performance. Our model parameter analysis has shown that root reinforcement, in conjunction with soil depth, transmissivity and soil cohesion, are the key parameters to predict slope stability in the studied mountainous regions. A major focus of the presented work was the assessment of the model's ability to study scenarios of vegetation distribution. Comparison of different scenarios ranging from uniform to single-tree detection-based vegetation clearly showed that the model output, in terms of shallow landslide probability, is highly sensitive to the spatial distribution of vegetation. Accordingly, the model is fit for future scenario analysis, including e.g. different protection forest management scenarios. In fact, a single-tree scale model parameterization provides the opportunity to run hypothetical vegetation scenarios reflecting on small scale managements strategies. Future improvements in the hydrological approach, concerning a more catchment based approach to compute saturation degree, will likely further improve the performance of SfM.



520 Appendix A: Appendix

Table A1. The hybrid Table for the soil cohesion and angle of internal friction for the relevant set of USCS soil classes. Derived from laboratory experiments (VSS-Kommission, 1998; Dysli and Rybisar, 1992) and combined in this research to exclude values that seemed unrealistic.

USCS soil class	Mean soil cohesion	Std. dev. soil cohesion	Mean friction angle	Std. dev. friction angle
SM	0	0	34.5	5.0
CL-ML	0.4	1.3	32.7	4.8
GM	0.0	0.0	35.0	5.0
GC-GM	5.0	5.0	33.0	3.0
CL	6.2	11.3	27.1	5.2
OL	2.5	5.0	32.8	2.2
GC	20.0	52.9	31.4	3.6

Code availability. The source code of SfM, written in R, is available on Github (FeikovZ/SfM). Additional code used to prepare input data is referenced in the text.

Data availability. All data used in this research is open data. The topographical data and the landslide inventory as used in this research are published on Zenodo

525 *Author contributions.* A.A. collected the landslide inventory and made it ready for use. D.C. and M.S. developed the basic concept of SlideforMap. L.D. contributed in the further development. F.Z. executed further development, the sensitivity analysis and testing. F.Z. is the main writer. B.S. L.D. C.P. A.A. and M.S. revised the text. C.P. and M.S. organized funds.

Competing interests. The authors declare no conflict of interest.

530 *Disclaimer.* The shallow landslide probability maps generated by SfM are a guideline and should be interpreted by an expert before application.

<https://doi.org/10.5194/nhess-2021-140>
Preprint. Discussion started: 25 May 2021
© Author(s) 2021. CC BY 4.0 License.



Acknowledgements. We thank the STEC (Smarter Targeting of Erosion Control) project by the Ministry of Business, Innovation and Employment of New Zealand for the financial support.



References

- 535 Askarinejad, A., Casini, F., Bischof, P., Beck, A., and Springman, S. M.: Rainfall induced instabilities: a field experiment on a silty sand slope in northern Switzerland, *rivista italiana di geotecnica*, pp. 50–71, <http://www.associazionegeotecnica.it/ig/archivio>, 2012.
- Askarinejad, A., Akca, D., and Springman, S. M.: Precursors of instability in a natural slope due to rainfall: a full-scale experiment, *Landslides*, 15, 1745–1759, <https://doi.org/10.1007/s10346-018-0994-0>, 2018.
- Badoux, A., Andres, N., Techel, F., and Hegg, C.: Natural hazard fatalities in Switzerland from 1946 to 2015, *Natural Hazards and Earth System Sciences*, 16, 2747–2768, <https://doi.org/10.5194/nhess-16-2747-2016>, 2016.
- 540 Baeza, C. and Corominas, J.: Assessment of shallow landslide susceptibility by means of multivariate statistical techniques, *Earth Surface Processes and Landforms*, 26, 1251–1263, <https://doi.org/10.1002/esp.263>, 2001.
- Bárdossy, A.: Calibration of hydrological model parameters for ungauged catchments, *Hydrology and Earth System Sciences*, 11, 703–710, <https://doi.org/10.5194/hess-11-703-2007>, 2007.
- Beven, K. and Freer, J.: A dynamic topmodel, *Hydrological Processes*, 15, 1993–2011, <https://doi.org/10.1002/hyp.252>, 2001.
- 545 Beven, K. J. and Kirkby, M. J.: A physically based, variable contributing area model of basin hydrology, *Hydrological Sciences Bulletin*, 24, 43–69, <https://doi.org/10.1080/02626667909491834>, 1979.
- Blazkova, S., Beven, K., Tacheci, P., and Kulasova, A.: Testing the distributed water table predictions of TOPMODEL (allowing for uncertainty in model calibration): The death of TOPMODEL?, *Water Resources Research*, 38, 39–1–39–11, <https://doi.org/10.1029/2001wr000912>, 2002.
- 550 Bodner, G., Leitner, D., and Kaul, H. P.: Coarse and fine root plants affect pore size distributions differently, *Plant and Soil*, 380, 133–151, <https://doi.org/10.1007/s11104-014-2079-8>, 2014.
- Bordoni, M., Meisina, C., Valentino, R., Lu, N., Bittelli, M., and Chersich, S.: Hydrological factors affecting rainfall-induced shallow landslides: From the field monitoring to a simplified slope stability analysis, *Engineering Geology*, 193, 19–37, <https://doi.org/10.1016/j.enggeo.2015.04.006>, 2015.
- 555 Borga, M., Dalla Fontana, G., Gregoretti, C., and Marchi, L.: Assessment of shallow landsliding by using a physically based model of hillslope stability, *Hydrological Processes*, 16, 2833–2851, <https://doi.org/10.1002/hyp.1074>, 2002.
- Cislaghi, A., Rigon, E., Lenzi, M. A., and Bischetti, G. B.: A probabilistic multidimensional approach to quantify large wood recruitment from hillslopes in mountainous-forested catchments, *Geomorphology*, 306, 108–127, <https://doi.org/https://doi.org/10.1016/j.geomorph.2018.01.009>, <https://www.sciencedirect.com/science/article/pii/S0169555X1830014X>,
- 560 2018.
- Cohen, D. and Schwarz, M.: Tree-root control of shallow landslides, *Earth Surface Dynamics*, 5, 451–477, <https://doi.org/10.5194/esurf-5-451-2017>, 2017.
- Cohen, D., Lehmann, P., and Or, D.: Fiber bundle model for multiscale modeling of hydromechanical triggering of shallow landslides, *Water Resources Research*, 45, 1–20, <https://doi.org/10.1029/2009WR007889>, 2009.
- 565 Corominas, J., van Westen, C., Frattini, P., Cascini, L., Malet, J. P., Fotopoulou, S., Catani, F., Van Den Eeckhaut, M., Mavrouli, O., Agliardi, F., Pitalakis, K., Winter, M. G., Pastor, M., Ferlisi, S., Tofani, V., Hervás, J., and Smith, J. T.: Recommendations for the quantitative analysis of landslide risk, *Bulletin of Engineering Geology and the Environment*, 73, 209–263, <https://doi.org/10.1007/s10064-013-0538-8>, 2014.
- Day, R. W.: State of the art: Limit equilibrium and finite-element analysis of slopes, *Journal of Geotechnical and Geoenvironmental Engineering*, 123, 894, [https://doi.org/10.1061/\(ASCE\)1090-0241\(1997\)123:9\(894\)](https://doi.org/10.1061/(ASCE)1090-0241(1997)123:9(894)), 1997.



- 570 Dazio, E. P. R., Conedera, M., and Schwarz, M.: Impact of different chestnut coppice managements on root reinforcement and shallow landslide susceptibility, *Forest Ecology and Management*, 417, 63–76, <https://doi.org/10.1016/j.foreco.2018.02.031>, <https://doi.org/10.1016/j.foreco.2018.02.031>, 2018.
- Dietrich, W. E. and Montgomery, D. R.: SHALSTAB: a digital terrainmodel for mapping shallow landslide potential., Tech. rep., NCASI (NationalCouncil of the Paper Industry for Air and Stream Improvement), 1998.
- 575 D’Odorico, P. and Fagherazzi, S.: A probabilistic model of rainfall-triggered shallow landslides in hollows: A long-term analysis, *Water Resources Research*, 39, 1–14, <https://doi.org/10.1029/2002WR001595>, 2003.
- Dorren, L.: FINT – Find individual trees. User manual., ecorisQ paper (www.ecorisq.org), p. 5 p, 2017.
- Dorren, L. and Sandri, A.: Landslide risk mapping for the entire Swiss national road network, *Landslide Processes*, pp. 277–281, <http://eost.u-strasbg.fr/omiv/Landslide{ }Processes{ }Conference/Dorren{ }et{ }al.pdf>, 2009.
- 580 Dysli, M. and Rybisar, J.: Statistique sur les caractéristiques des sols suisses- Statistische Behandlung der Kennwerte der Schweizer Boeden., Bundesamt fuer Strassenbau, 1992.
- Eysn, L., Hollaus, M., Lindberg, E., Berger, F., Monnet, J. M., Dalponte, M., Kobal, M., Pellegrini, M., Lingua, E., Mongus, D., and Pfeifer, N.: A benchmark of lidar-based single tree detection methods using heterogeneous forest data from the Alpine Space, *Forests*, 6, 1721–1747, <https://doi.org/10.3390/f6051721>, 2015.
- 585 Fawcett, T.: An introduction to ROC analysis, *Pattern Recognition Letters*, <https://doi.org/10.1016/j.patrec.2005.10.010>, 2006.
- Freeze, R. A. and Cherry, J. A.: *Groundwater*, No. 629.1 F7, 1979.
- Frei, C., Isotta, F., and Schwanbeck, J.: Mean Precipitation 1981-2010, in: *Hydrological Atlas of Switzerland*, Geographisches Institut der Universität Bern, 2020.
- Gehring, E., Conedera, M., Maringer, J., Giadrossich, F., Guastini, E., and Schwarz, M.: Shallow landslide disposition in burnt European beech (*Fagus sylvatica* L.) forests, *Scientific Reports*, 9, 1–11, <https://doi.org/10.1038/s41598-019-45073-7>, 2019.
- 590 González-Ollauri, A. and Mickovski, S. B.: Integrated Model for the Hydro-Mechanical Effects of Vegetation Against Shallow Landslides, *EQA - International Journal of Environmental Quality*, 13, 37–59, <https://doi.org/10.6092/issn.2281-4485/4535>, <https://eqa.unibo.it/article/view/4535/4013>, 2014.
- Grabs, T., Seibert, J., Bishop, K., and Laudon, H.: Modeling spatial patterns of saturated areas: A comparison of the topographic wetness index and a dynamic distributed model, *Journal of Hydrology*, 373, 15–23, <https://doi.org/10.1016/j.jhydrol.2009.03.031>, <http://dx.doi.org/10.1016/j.jhydrol.2009.03.031>, 2009.
- 595 Greenway, D. R.: Vegetation and slope stability, *Slope Stabilization*, pp. 187–23, 1987.
- HADES: https://hydrologischeratlas.ch/downloads/01/content/Text_Tafel24.de.pdf, 2020.
- Hawley, J. and Dymond, J.: How much do trees reduce landsliding?, *Journal of Soil&Water Conservation*, 43, 495–498, 1988.
- 600 Iida, T.: A stochastic hydro-geomorphological model for shallow landsliding due to rainstorm, *Catena*, 34, 293–313, [https://doi.org/10.1016/S0341-8162\(98\)00093-9](https://doi.org/10.1016/S0341-8162(98)00093-9), 1999.
- Iverson, R. M.: Landslide triggering by rain infiltration, *Water Resources Research*, 36, 1897–1910, <https://doi.org/10.1029/2000WR900090>, <http://doi.wiley.com/10.1029/2000WR900090>, 2000.
- Jensen, H., Lang, H., and Rinderknecht, J.: Extreme Punktregen unterschiedlicher Dauer und Wiederkehrperioden 1901-1970, Tafel 2.4., in: 605 *Hydrologischer Atlas der Schweiz*, Geographisches Institut der Universität Bern, 1997.
- Johnson, N. L. and Kotz, S.: *Continuous univariate distributions*, Houghton Mifflin, Boston, 1970.



- Kjekstad, O. and Highland, L.: Economic and Social Impacts of Landslides, *Landslides – Disaster Risk Reduction*, 30, 573–587, https://link.springer.com/content/pdf/10.1007/978-3-540-69970-5_{_}30.pdf, 2009.
- 610 Korpela, I., Dahlin, B., Schäfer, H., Bruun, E., Haapaniemi, F., Honkasalo, J., Ilvesniemi, S., Kuutti, V., Linkosalmi, M., Mustonen, J., Salo, M., Suomi, O., and Virtanen, H.: Single-tree forest inventory using lidar and aerial images for 3D treetop positioning, species recognition, height and crown width estimation, *International Archives of the Photogrammetry, Remote Sensing and Spatial Information Sciences*, 36, 227–233, 2007.
- Lehmann, P., Gambazzi, F., Suski, B., Baron, L., Askarinejad, A., Springman, S. M., Holliger, K., and Or, D.: Evolution of soil wetting patterns preceding a hydrologically induced landslide inferred from electrical resistivity survey and point measurements of volumetric water content and pore water pressure, *Water Resources Research*, 49, 7992–8004, <https://doi.org/10.1002/2013WR014560>, 2013.
- 615 Leonarduzzi, E., Molnar, P., and McArdell, B. W.: Predictive performance of rainfall thresholds for shallow landslides in Switzerland from gridded daily data, *Water Resources Research*, 53, 6612–6625, <https://doi.org/10.1002/2017WR021044>, 2017.
- Li, W. C., Lee, L. M., Cai, H., Li, H. J., Dai, F. C., and Wang, M. L.: Combined roles of saturated permeability and rainfall characteristics on surficial failure of homogeneous soil slope, *Engineering Geology*, 153, 105–113, <https://doi.org/10.1016/j.enggeo.2012.11.017>, <http://dx.doi.org/10.1016/j.enggeo.2012.11.017>, 2013.
- 620 Malamud, B., Turcotte, D., Guzzetti, F., and Reichenbach, P.: Landslide inventories and their statistical properties, *Earth Surface Processes and Landforms*, 29, 687–711, <https://doi.org/10.1002/esp.1064>, 2004.
- McKay, M. D., Beckman, R. J., and Conover, W. J.: Comparison of three methods for selecting values of input variables in the analysis of output from a computer code, *Technometrics*, 21, 239–245, <https://doi.org/10.1080/00401706.1979.10489755>, 1979.
- 625 Menk, J., Dorren, L., Heinzl, J., Marty, M., and Huber, M.: Evaluation automatischer Einzelbaumerkennung aus luftgestützten Laserscanning-Daten, *Schweizerische Zeitschrift für Forstwesen*, 168, 151–159, <https://doi.org/10.3188/szf.2017.0151>, 2017.
- Metz, C. E.: Basic principles of ROC analysis., *Seminars in nuclear medicine*, 8, 283–298, [https://doi.org/http://dx.doi.org/10.1016/S0001-2998\(78\)80014-2](https://doi.org/http://dx.doi.org/10.1016/S0001-2998(78)80014-2), 1978.
- Montgomery, D. R. and Dietrich, W. E.: A physically based model for the topographic control on shallow landsliding, *Water Resources Research*, 30, 1153–1171, <https://doi.org/10.1029/93WR02979>, 1994.
- 630 Moos, C., Bebi, P., Graf, F., Mattli, J., Rickli, C., and Schwarz, M.: How does forest structure affect root reinforcement and susceptibility to shallow landslides?, *Earth Surface Processes and Landforms*, 41, 951–960, <https://doi.org/10.1002/esp.3887>, 2016.
- Mosley, M. P.: Subsurface flow velocities through selected forest soils, South Island, New Zealand, *Journal of Hydrology*, 55, 65–92, [https://doi.org/10.1016/0022-1694\(82\)90121-4](https://doi.org/10.1016/0022-1694(82)90121-4), 1982.
- 635 Munich RE: Relevant hydrological events worldwide 1980 - 2018, NatCatService, 2018.
- O’Callaghan, J. F. and Mark, D. M.: The Extraction of Drainage Networks from Digital Elevation Data, *Computer Vision, Graphics and Image Processing*, 28, 323–344, [https://doi.org/10.1016/0734-189X\(89\)90053-4](https://doi.org/10.1016/0734-189X(89)90053-4), 1984.
- O’Loughlin, E. M.: Prediction of Surface Saturation Zones in Natural catchments by Topographic Analysis, *Water resources research*, 22, 794–804, 1986.
- 640 Park, H. J., Lee, J. H., and Woo, I.: Assessment of rainfall-induced shallow landslide susceptibility using a GIS-based probabilistic approach, *Engineering Geology*, 161, 1–15, <https://doi.org/10.1016/j.enggeo.2013.04.011>, <http://dx.doi.org/10.1016/j.enggeo.2013.04.011>, 2013.
- Price, B., Gomez, A., Mathys, L., Gardi, O., Schellenberger, A., Ginzler, C., and Thürig, E.: Tree biomass in the Swiss landscape: nationwide modelling for improved accounting for forest and non-forest trees, *Environmental Monitoring and Assessment*, 189, <https://doi.org/10.1007/s10661-017-5816-7>, 2017.



- 645 Reinhold, S., Medicus, G., Fellin, W., and Zangerl, C.: The influence of deforestation on slope (In-) stability, *Austrian Journal of Earth Sciences*, 102, 90–99, <https://doi.org/10.1139/t01-031>, 2009.
- Rickli, C. and Graf, F.: Effects of forests on shallow landslides – case studies in Switzerland, *Forest Snow and Landscape Research*, 44, 33–44, <http://www.issw.ch/wsl/publikationen/pdf/9696.pdf>, 2009.
- Rickli, C., Graf, F., Bebi, P., Bast, A., Loupt, B., and McARDell, B.: Schützt der Wald vor Rutschungen? Hinweise aus der WSL-
650 Rutschungsdatenbank, *Schweizerische Zeitschrift für Forstwesen*, 170, 310–317, <https://doi.org/10.3188/szf.2019.0310>, 2019.
- Roering, J., Schmidt, K. M., Stock, J. D., Dietrich, W. E., and Montgomery, D. R.: Shallow landsliding, root reinforcement, and the spatial distribution of trees in the Oregon Coast Range, *Canada Geotechnical Journal*, 40, 237–253, 2003.
- Salvatici, T., Tofani, V., Rossi, G., D’Ambrosio, M., Tacconi Stefanelli, C., Benedetta Masi, E., Rosi, A., Pazzi, V., Vannocci, P., Petrolo, M.,
655 Catani, F., Ratto, S., Stevenin, H., and Casagli, N.: Application of a physically based model to forecast shallow landslides at a regional scale, *Natural Hazards and Earth System Sciences*, 18, 1919–1935, <https://doi.org/10.5194/nhess-18-1919-2018>, 2018.
- Schaefli, B. and Gupta, H.: Do Nash values have value, *Hydrological Processes*, 21, 2075–2080, <https://doi.org/10.1002/hyp>, <http://jamsb.austms.org.au/courses/CSC2408/semester3/resources/ldp/abs-guide.pdf>, 2007.
- Schwarz, M., Preti, F., Giadrossich, F., Lehmann, P., and Or, D.: Quantifying the role of vegetation in slope stability: A case study in Tuscany (Italy), *Ecological Engineering*, 36, 285–291, <https://doi.org/10.1016/j.ecoleng.2009.06.014>, 2010.
- 660 Schwarz, M., Rist, A., Cohen, D., Giadrossich, F., Egorov, P., Büttner, D., Stolz, M., and Thormann, J. J.: Root reinforcement of soils under compression, *Journal of Geophysical Research F: Earth Surface*, 120, 2103–2120, <https://doi.org/10.1002/2015JF003632>, 2015.
- Sidle, R. C.: A Theoretical Model of the Effects of Timber harvesting on Slope Stability, *Water Resources Research*, 28, 1897–1910, 1992.
- Swiss Re Institute: Natural catastrophes and man-made disasters in 2018: “secondary” perils on the frontline., *Sigma*, 2, 1–36, 2019.
- Swisstopo: SWISSIMAGE. Luftbilder Level 2 (25 cm) Wabern: Bern, 2017.
- 665 Swisstopo: SwissALTI3D Das hoch auf-gelöste Terrainmodell der Schweiz, 2018.
- Swisstopo: Switzerland forest cover map; <https://shop.swisstopo.admin.ch/de/products/maps/national/vector/smv25>, 2020.
- Torres, R., Dietrich, W. E., Montgomery, D. R., Anderson, S. P., and Loague, K.: Unsaturated zone processes and the hydrologic response of a steep, unchanneled catchment, *Water Resources Research*, 34, 1865–1879, <https://doi.org/10.1029/98WR01140>, 1998.
- Varnes, D. J.: Slope Movement Types and Processes, Special report, 176, 11–33, <https://doi.org/10.1016/j.mser.2018.11.001>, 1978.
- 670 Vergani, C., Schwarz, M., Cohen, D., Thormann, J., and Bischetti, G.: Effects of root tensile force and diameter distribution variability on root reinforcement in the Swiss and Italian Alps, *Canadian Journal of Forest Research*, 44, 1426–1440, <https://doi.org/10.1139/cjfr-2014-0095>, <http://www.nrcresearchpress.com/doi/abs/10.1139/cjfr-2014-0095>{#}.VPm77k0tHoo, 2014.
- VSS-Kommission: Schweizer Norm, 670 010b, Tech. rep., Schweizer Norm, 1998.
- Weiler, M. and Naef, F.: An experimental tracer study of the role of macropores in infiltration in grassland soils, *Hydrological Processes*, 17,
675 477–493, <https://doi.org/10.1002/hyp.1136>, 2003.
- Wickenkamp, I., Huisman, J. A., Bogena, H. R., Lin, H. S., and Vereecken, H.: Spatial and temporal occurrence of preferential flow in a forested headwater catchment, *Journal of Hydrology*, 534, 139–149, <https://doi.org/10.1016/j.jhydrol.2015.12.050>, <http://dx.doi.org/10.1016/j.jhydrol.2015.12.050>, 2016.
- Wu, T., McKinnel, W. P., and Swanston, D. N.: Strength of tree roots and landslides on Prince of Wales Island, Alaska, *Canada Geotechnical Journal*, pp. 19–33, 1978.
- 680



- Xu, C., Xu, X., Dai, F., and Saraf, A. K.: Comparison of different models for susceptibility mapping of earthquake triggered landslides related with the 2008 Wenchuan earthquake in China, *Computers and Geosciences*, 46, 317–329, <https://doi.org/10.1016/j.cageo.2012.01.002>, <http://dx.doi.org/10.1016/j.cageo.2012.01.002>, 2012.
- Zevenbergen, L. and Thorne, C.: Quantitative analysis of land surface topography, *Earth Surface Processes and Landforms*, 12, 47–56, 1987.
- 685 Zhang, S., Zhao, L., Delgado-Tellez, R., and Bao, H.: A physics-based probabilistic forecasting model for rainfall-induced shallow landslides at regional scale, *Natural Hazards and Earth System Sciences*, 18, 969–982, <https://doi.org/10.5194/nhess-18-969-2018>, 2018.
- Zhu, H., Zhang, L. M., Xiao, T., and Li, X. Y.: Enhancement of slope stability by vegetation considering uncertainties in root distribution, *Computers and Geotechnics*, 85, 84–89, <https://doi.org/10.1016/j.compgeo.2016.12.027>, 2017.